TECHNICAL PAPER

Design and modeling of a multiband electrically coupled loop antenna for biomedical applications

Abdullah Muhammad Mahfouz[1] · Ali Ahmed Younis Ibraheem[1] · Osama M. Haraz[1]

Abstract

A triple-band Electrically Coupled Loop Antenna (ECLA) is designed to operate in the three standard bands for biomedical implantation purposes: Medical Implant Communications Services (MICS) (402–405 MHz), Wireless Medical Telecommunication Services (WMTS) (1395–1405 MHz) and Industrial, Scientific, and Medical (ISM) (2400–2480 MHz). An equivalent circuit is derived for the multiband ECLA based on simple equations relate the dimensions with the circuit parameters to get a good understanding of antenna operation as well as saving time in simulations. The proposed antenna size is $15 \times 13.8 \times 13$ mm^3 and simulated in a muscle phantom with size $100 \times 100 \times 100$ mm^3. The calculated peak realized gain values are -18, -30 and -33.3 dBi and the peak 10 g averaged Specific Absorption Rate (SAR) values are 11.59, 43.07 and 49.75 W/Kg for the three bands, respectively. A detuning study is carried out to ensure that the proposed antenna is robust against electrical properties variation thus it can be implanted in different tissues of different people in various health circumstances. Two antenna prototypes have been fabricated and tested in a solution that mimics human tissue.

1 Introduction

A tremendous development is observed in treatment and diagnosis methods as well as remote health monitoring through the Implanted Medical Devices (IMDs) (Hall and Hao 2006). The main task of the IMDs is to acquire and transfer vital data wirelessly to take a quick decision to save the patient from the sudden ailments. Other functions have been proposed to improve the system performance such wake up control and energy harvesting so a multiband antenna is required to meet these specifications. The design frame of the IMDs is limited to some obstacles. They can be generally gathered in size and safety limitations in addition to quality and robustness demands. For a further discussion, the implanted device should be as small as possible for human comfort and thus reduces the size of the antenna as well. The reduction in the antenna size operating at a certain frequency leads to reduction in the radiated power.

To conserve the same radiated power, the fed power must be increased to compensate the loss in both the antenna and the dissipative medium surrounds the antenna. This leads to another two important parameters, safety and the battery lifetime.

Safety criterion is expressed by Specific Absorption Rate (SAR) averaged on mass of (1gm or 10gm) according to the following standards (1.6 W/Kg or 2 W/Kg), respectively. SAR is a parameter that measures how the human tissues influence by the radiated power. Battery lifetime is an important aspect, simply in case the battery is expired, the implanted system becomes dead meaning that there are useless pieces of metals and semiconductors in the body until the battery is changed which is completely against the patient's comfort.

Human tissues are considered dispersive dissipative dielectrics, then to guarantee antenna impedance matching in specific band it should achieve either sufficient amount of bandwidth to cover the possibilities of electrical properties changes which depends on antenna nearfield type either electric or magnetic.

Many of the antennas used for such implanted applications are electrically small antennas (ESAs). The characteristics of this type of antennas are low radiation efficiency, low directivity, roughly 1.5 dimensionless and

✉ Osama M. Haraz
o_haraz@aun.edu.eg

[1] Electrical Engineering Department, Faculty of Engineering, Assiut University, Assiut 71516, Egypt

low radiation resistance i.e. difficult to be matched to a 50 Ohm system. If the antenna is loaded by a high relative permittivity dielectric, the antenna impedance is enhanced to a considerable value which enables the antenna to be matched with a 50 Ohm system. ESA becomes easily matched at the same resonance frequency without load, but this comes from the loss in the dielectric medium and the trapped power in it hence the radiation efficiency will severely decrease and the antenna gain (radiated power outside the phantom divided by accepted power) becomes friction from one or goes to negative values in dB.

Although small dimensions imply low radiating characteristics of the antenna but the magnetic dipole antenna has superior performance than electric dipole antenna as reported in Geyi (2003). A mathematical derivation has been introduced to calculate the quality factor Q for small antennas. It has been proved that the Q of a small loop antenna is about three times lower than that of a small dipole for the same radian sphere ka, that implies two important features of the small loop antennas which are higher radiation efficiency and larger bandwidth than electric dipole. The nearfield coupled to the small loops is mainly magnetic (Balanis 2016). This ensures safety and robustness requirements. For safety, SAR depends on the bulk conductivity of the surrounding medium and the electric field values in it which is overwhelmed by the magnetic field in the nearfield region. The antenna matching is controlled by the total radiated field and the coupled nearfield as well. As known the trapped field is represented by reactive element and the useful radiated field in addition to antenna loss are modelled by resistors. Because the nearfield of the loop antennas is mainly magnetic, they are distinguished with high immunity to detuning which implies robust performance in a time-variant media such as human tissue.

The stipulated frequency bands dedicated for Wireless Body Area Network (WBAN) cover three major bands: Medical Implant Communications Services (MICS) 402–405 MHz, Wireless Medical Telecommunication Services (WMTS) 1395–1400 MHz and Industrial, Scientific, Medical (ISM) 2400–2480 MHz. There are different definitions for these bands but the mentioned frequency limits are globally accepted for different communication scenarios. The proposed antenna is designed to use these frequency bands for data telemetry, Wireless Power Transfer (WPT) and system wake up control respectively.

Recently, a promising radiating structure has been introduced to fulfill the implanted system requirements. This structure may be generally categorized under loop antennas class, but it is not a planar loop, lies in a plane, it is a 3D loop, i.e. it has a depth parallel to the loop axis as shown in Fig. 1a. This loop is electrically excited via capacitive coupling between feeder head and the loop

starter. This type is introduced as a dual of PIFA and is called Electrically Coupled Loop Antenna (ECLA) (Manteghi 2013). It is tuned to resonate at MICS band with two versions (Ibraheem et al. 2014). The first one has a size of $14 \times 13.5 \times 13 mm^3$ which corresponds to $0.02\lambda \times 0.018\lambda \times 0.017\lambda$. The second is a miniaturized version of the former design with dimensions $5 \times 5 \times 3 mm^3$. It is also tuned to operate at two bands with the same dimensions for both versions (Akbarpour and Somayyeh 2017). These dimensions reveal that the ECLA for that design is electrically small antenna.

In this paper, a circuit model for the ECLA is introduced for both single and dual band structures. Through this model a design of the triple band prototype is proposed, designed, manufactured and tested experimentally. The extraction of circuit parameters values depends mainly on two aspects:—First, the structure is electrically small so there is no need to consider distributed models such as transmission line model. Second, the experimental trials using full wave simulators. The rest of the paper starts with Sect. 2 which presents a general description to the circuit model of the single band ECLA and how to evaluate the circuit elements with a nominal example. Then, the dual band ECLA is reviewed with the corresponding equivalent circuit in Sect. 3. The medium loading is studied and taken into account in the circuit modeling in Sect. 4. The tri-band ECLA is explained in Sect. 5 with the corresponding resonance elements. Section 6 introduces an experimental verification and results. Conclusions are given in Sect. 7.

2 ECLA circuit model

2.1 Descriptive explanation

The resonance of an electrically small antenna ESA is usually modeled by parallel RLC circuit. This is because the ESA is either a magnetic dipole modelled by an inductor or an electric dipole modeled by a capacitor. To achieve matching a reactive element is added. It is a capacitor in case the ESA is a magnetic dipole and an inductor if the ESA is an electric dipole. The resistor of the parallel tank indicates the loss and the radiating power amount. Although the metallic losses are usually very small, in milliohms, they cannot be neglected since radiation resistance may take values in the same range. Loss resistance can be calculated simply using (1) taking into account the skin effect.

$$R_{Loss} = l/w\sqrt{\pi f \mu / \sigma} \tag{1}$$

Fig. 1 **a** ECLA structure and **b** Elevation view the arrows represents current path through metal and the electric field between metallic sheets

(a)   (b)
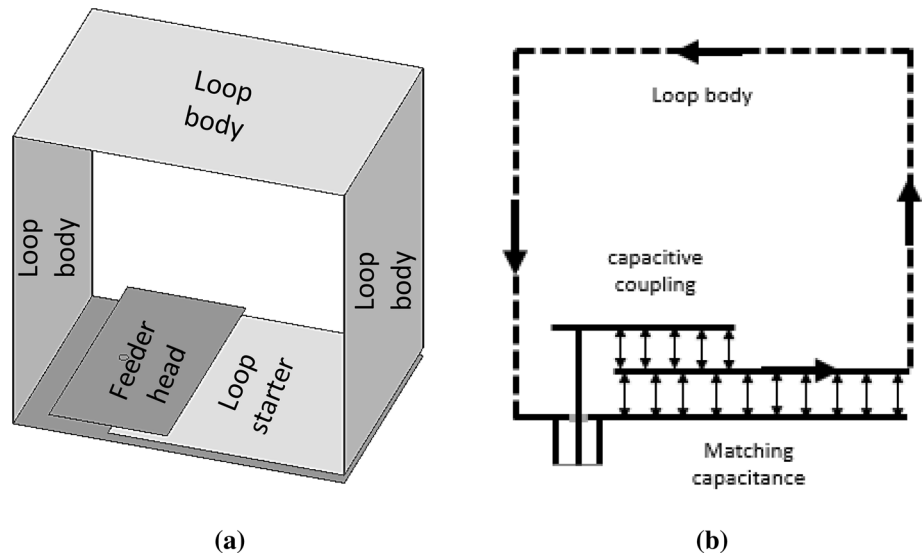
Radiation resistance of ESA can be calculated using (2) for both electric and magnetic dipoles assuming constant current distributions. (Ramo and Whinnery 2008).

$$R_r = 80\pi^2(l/\lambda)^2 \tag{2a}$$

$$R_r = 20\pi^2(C/\lambda)^4 \tag{2b}$$

where l, C represent the length of the dipole and the circumference of the loop respectively.

Radiation resistance can be connected in series with inductor representing a small loop or may be replaced by its conductance to be connected in parallel with a capacitor representing an electric dipole as suggested by Wheeler in (1947). ECLA may be treated and modeled by the same procedure. The 3D loop may be considered as an inductor in series with a resistance represents the radiated power and loss.

Input impedance of the loop can be pure resistive through a two parallel plates capacitor formed by the loop starter part and the ground sheet. The proposed equivalent circuit for the single band ECLA is depicted in Fig. 2a. It consists of two main parts, i.e. resonance elements and coupling elements. Resonance elements are L_r, R_A and C_r. Coupling elements are C_C and L_C where C_C dominates at the low frequencies unlike L_C which dominates at the high frequencies.

The features of this antenna may be pronounced by investigating the ECLA response over a large band covers from 0.1 up to 4 GHz as illustrated in Fig. 2b. It is worthy to mention that the ECLA was simulated in free space without any dielectric loading. The dimensions are tabulated in the following section. The impedance value of the antenna at the resonance is resistive and equal to $L_r/(R_A C_r)$ so the response has large limits exceeds $\pm 3.5 K\Omega$ but it is intentionally bounded between $\pm 100\Omega$ in

display for convenience. Also the resonance bandwidth is very small. These effects are due to the antenna losses in addition to low radiated power, in other words the series resistance R_A has a low value. At low frequencies, below resonance, the imaginary part of the antenna goes to large negative values, contrary to what expected, indicating that a capacitance existence overwhelms the conventional resonance circuit response so, the capacitive coupling between feeder head and the loop starter can be modeled by a capacitor connected in series with the resonance circuit. It should also be noted that, the imaginary part has a positive slope over all studied band except the resonance band. At first glance, this seems normal but at relatively high frequencies the curve behaves as a linear function. This suggests attaching a series inductance with the coupling capacitor. It may be guessed to occur due to the loop starter.

2.2 Parameter extraction

It is clear that capacitors take the parallel plate structure with rectangular shape but it is not preferable to use the simple formula to estimate capacitance value since it neglects fringing effects. For more accurate results, (3) may be used instead according to Hosseini et al. (2007).

$$\frac{C}{\varepsilon_r \varepsilon_0} = \frac{WL}{d}\left[1 + \frac{d}{\pi W}\left(1 + \ln\left(\frac{2\pi W}{d}\right)\right)\right]$$
$$\left[1 + \frac{d}{\pi L}\left(1 + \ln\left(\frac{2\pi L}{d}\right)\right)\right] \tag{3}$$

where, WL d and ε_r represent plate area, separation between two parallel plates and the relative permittivity of the dielectric separator, respectively. The loop has depth so it is considered as a series of planar sheets connected
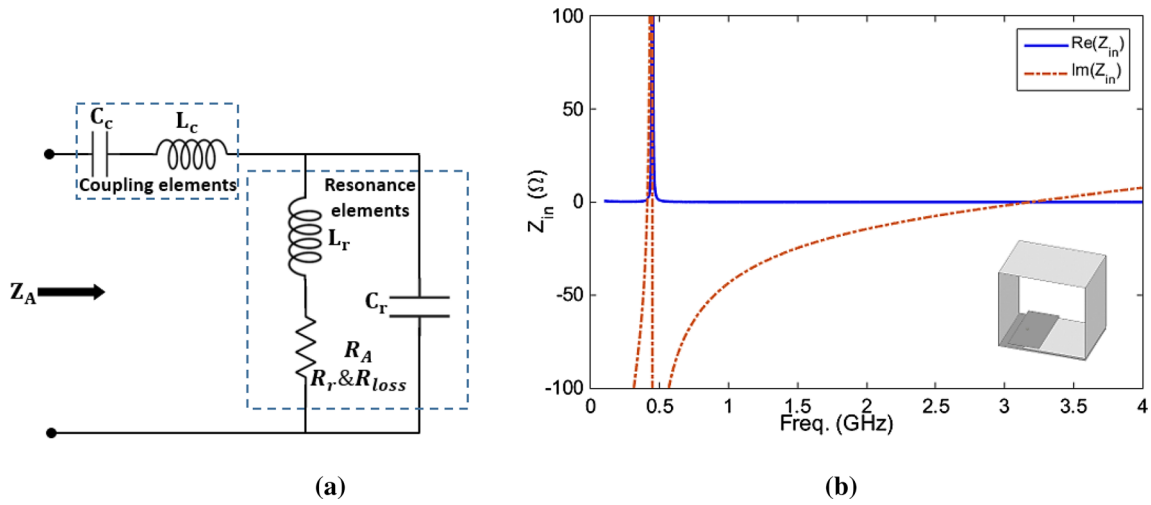
Fig. 2 **a** Equivalent Circuit. **b** Full wave simulation response

together. The inductance of a planar sheet may be calculated through the ribbon inductance formula (4) stated in Khan (2014).

$$L = 5.08 \times 10^{-3} l \left[\ln \left(\frac{l}{w+t} \right) + 1.19 + 0.022 \left(\frac{w+t}{l} \right) \right]$$

(4)

where l, w and t represent length, width and metal thickness of the ribbon or sheet successively. Dimensions in this equation must be entered in mils to give the inductance in nHs. The coupling inductance L_c is formed by the loop starter part under the feeder head. As for the resonance inductance L_r, it is formed by the loop body in addition to the remainder of the loop starter. It should be noted that the loop starter inductance will be calculated at first then it would be divided into two components relatively.
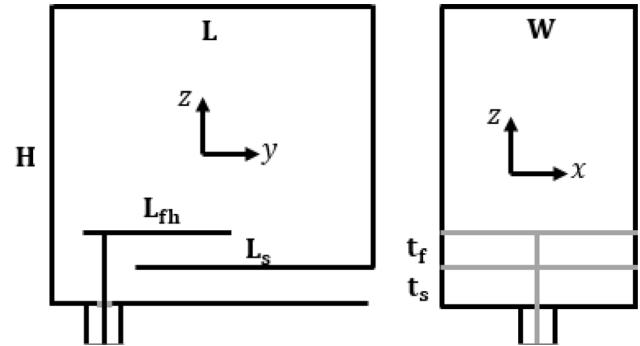

Fig. 3 Dimension declaration elevation and side views

2.3 Nominal example

Table 1 shows the dimensions for a single band ECLA as in Fig. 3 and the corresponding circuit elements values.

Figure 4 shows the impedance responses of the full wave simulation and the corresponding equivalent circuit.

Table 1 Dimensions and circuit parameters

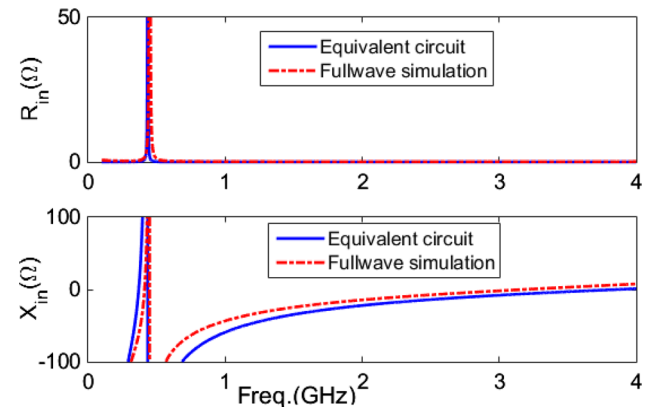| Dimension	Value (mm)	Element	Value
L	14.0	$C_c (pF)$	3.69
W	10.0	$L_c (nH)$	0.64
H	13.5	$C_r (pF)$	9.69
L_{fh}	5.0	$L_r (nH)$	13.8
L_s	10.0	$R_r (\Omega)$	0.00435
t_s	0.3556	$R_{loss} (\Omega)$	0.00825 $\sqrt{f}$,
t_f	0.3556		f IN GHZ
t_{cu}	0.18		
t_{Teflon}	3.0		
x_f	1.5		

Fig. 4 Impedance responses of both equivalent circuit and full wave simulation

There are some deviations between two responses since some parameters have not been taken into account such the dielectric loss, so we note the bandwidth of the full wave simulation seems less larger than the equivalent circuit response. Also, the radiation resistance is considered to have a constant value, at the resonance, with frequency because the resonance capacitor dominates at the high frequency and the tank impedance will go to zero. However, the extracted paramteres can be tuned to get equivalent circuit with highly similar response like the ECLA reponse but we settle for/ceases to descriptive and simple understanding of the ECLA behaviour.

3 Dual band ECLA

A dual band implanted antenna is suggested to achieve two functions separately for both bands. The first lower band is assigned for biomedical telemetry while the other high range is used to control the implanted device. In (Akbarpour and Somayyeh 2017) the dual band ECLA is introduced. It was also inspired from the dual band PIFA using the duality between both structures. It is possible to see this duality using circuit modeling provided that the parts which excite the another high band can be determined. The dual band ECLA is shown in Fig. 5. The dashed line represents the metal sheet that caused the high band excitation. From the circuit model point of view it represents the inductance of the resonance circuit of the higher band. The tank capacitor comes from the trapped field between the added sheet and the feeder head as presented in Fig. 5.

The separation between the metalic sheet and the loop starter is relatively small doesn't exceed 2 mm so the flux

due to the current passes through both the metalic sheet and the loop stareter part below it roughly vanishes consequently, the inductance of the upper band comes from the metalic sheet remainder above the feeder head and less excess depends on the height of the high band sheet. Both dual band ECLA and higher band exciter, shown in Fig. 5, are simulated. It is clear that the equivalent circuit of the high band exciter is the same as the single band ECLA shown in Fig. 2a. The circuit elements can be deduced follwing the same relations in the previous section. Table 2 summerizes the resonance parameters of the higher band exciter shown in Fig. 5b.

For the sake of simplification, the resistance values are taken the same as in Table 1. The impedance response of the high band exciter is introduced in Fig. 6.

Because of resonance frequencies splaying, as for equivalent circuit each band has little effect on the other. Also the parts which responsible for each band excitation are different as illustrated in the previous figures, so the overall equivalent circuit can be considered as a series connection between a two parallel resonance circuits connected in series with the coupling circuit as shown in Fig. 7a.

Figure 7b presents the overall response without taking into account the loading effect, i.e. $\Delta Z = 0$ which represents the impedance excess due to loading as described later in the next section. The circuit elements values are presented in the above tables. The slight down shift to the upper resonance frequency may occur in the full wave simulation response due to the slight increase in the inductance of the higher band. In other words, the current which passes through the loop starter is divided between the loop body and the metalic sheet that means the flux
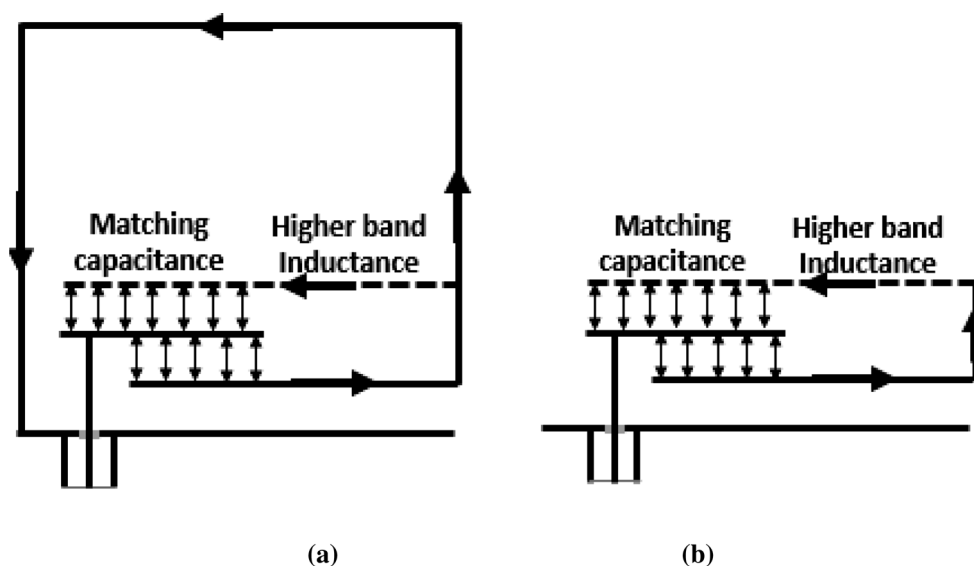

(a) (b)

Fig. 5 **a** Dual-band ECLA and **b** High band exciter

Table 2 Circuit parameters of the high band

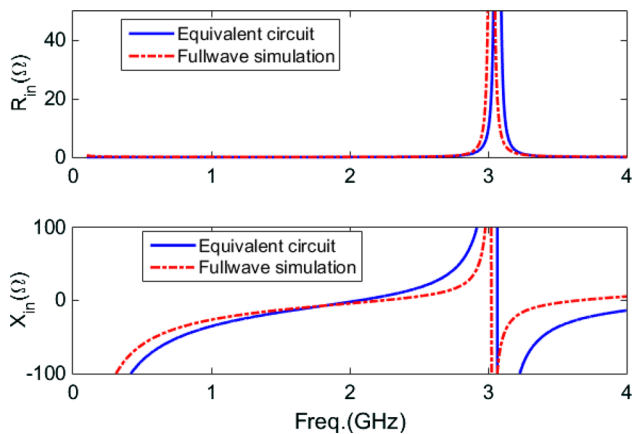| Element	$C_c (pF)$	$L_c (nH)$	$C_r (pF)$	$L_r (nH)$
Value	3.69	0.64	5.08	0.53

Fig. 6 Impedance responses of both equivalent circuit and full wave Simulation (high band exciter only)

between the loop starter and the metalic sheet is larger than the case of the high exciter existence alone.

4 Human tissue effect on the ECLA input impedance

The study of antenna performance immersed in dissipative media takes interest of researchers before 1950s to establish communication with underwater submarines or use it

for mining purposes (Wait 1957; Chen and King 1963; Turner 1959; Yan et al. 2013; Chao and Chung 1994; Ghosh et al. 2008; Manteghi and Ibraheem 2014). Recently, with the advent of implanted antennas, it is possible to take advantage of these studies since human tissues are dissipative dielectrics have characteristics look like sea water or ground. One of these studies was conducted by Wait (1957). The effect of loading dissipative dielectric on the input impedance of a small insulated circular loop was studied. The loop was assumed to carry uniform current along perimeter and is made from very thin wire. It was placed in the center of a sphere of vacuum surrounded by the finite conductivity medium. The loop fields are divided into a primary component because of loop itself and a secondary one because of the medium loading. The input impedance of the loop is expected to increase because of the new field component, so it is expressed as follows

$$Z = Z_0 + \Delta Z \tag{5}$$

where Z_0 represents the loop impedance in the free space and it was assumed to be known and ΔZ indicates to the excess due to finite vacuum size and denoted by

$$\Delta Z = j\omega\mu(S/a) \sum_{n=1}^{\infty} (T_n/(n(n+1)))(b/a)^{2n} \left[P_n^1(0)\right]^2 \tag{6}$$

where S is the loop area, a, b represent the vacuum sphere radius and the loop radius respectively and P_n^1 is the associated Legendre function of n degree and order 1. T_n is a coefficient which contains the dissipative medium parameters denoted by
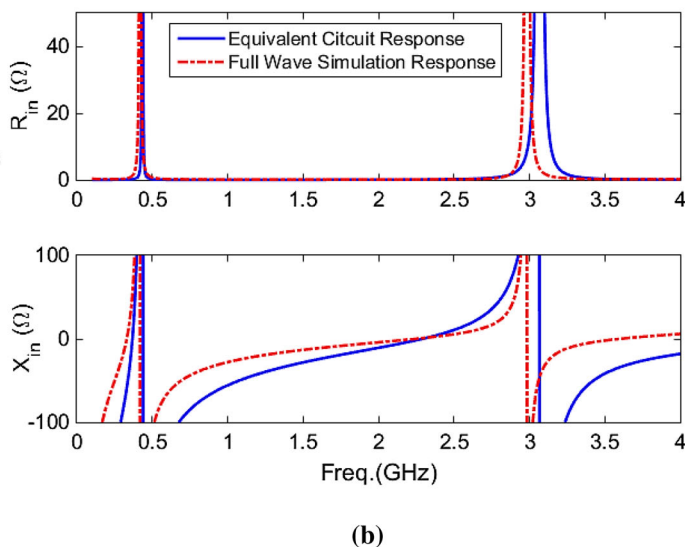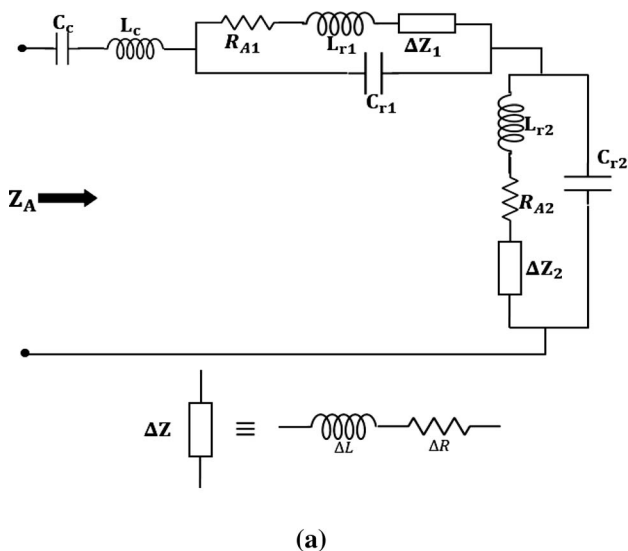

Fig. 7 **a** Equivalent circuit of the dual band ECLA and **b** Impedance response of both dual band equivalent circuit and full wave simulation

$$T_n = [(2n+1)/(n+1+\alpha_n)](b/a)^n \tag{7}$$

$$\alpha_n = \left[z + \left(\sum_{m=0}^{n} m a_m z^{-m}\right) / \left(\sum_{m=0}^{n} a_m z^{-m}\right)\right]_{z=\gamma a} \tag{8}$$

$$\gamma = \sqrt{j\omega\mu\sigma - \omega^2\mu\varepsilon} \tag{9}$$

$$a_m = (n+m)! 2^{-m} / [(n-m)! m!] \tag{10}$$

Despite the ECLA is a 3D loop and not a planar loop, this analysis can be applied on condition that it is electrically small. It is possible to approximate the geometry of the ECLA which has a parallelepiped shape coated by a layer of biocompatible insulating material to a small loop counterpart to be matched with the geometry suggested by Wait (1957). The insulating cube can be converted into a sphere that has the same cube volume with radius a_1 and the 3D loop is replaced by a circular loop with radius b_1 where its area equals 3D loop cross section area. As for the upper band radiator, it is not logical to consider the insulating sphere radius a_2 is the same as a_1 because there are different media covering it, not only the insulating layer but also the vacuum in addition to loop metal, so it is suggested to modify the value of a_2 to get similar response at the high band instead of changing the electrical properties of the surrounding medium. Table 3 shows the radii of the equivalent geometry. The impedance response of the dual-band ECLA coated by 3 mm Teflon sheet as a biocompatible material and immersed in a human tissue is displayed in Fig. 8. Figure 9 illustrates the electrical properties of the immersing medium according to Dielectric Properties of Body Tissues (1987). By investigating Figs. 7b and 8, we can conclude that the medium loading affects the position of the resonance frequency, it pulled it down, due to inductive behavior of ΔZ. Also, there is excess in the series resistance due to medium dissipation that arises in the decreasing of the input impedance real part at resonance.
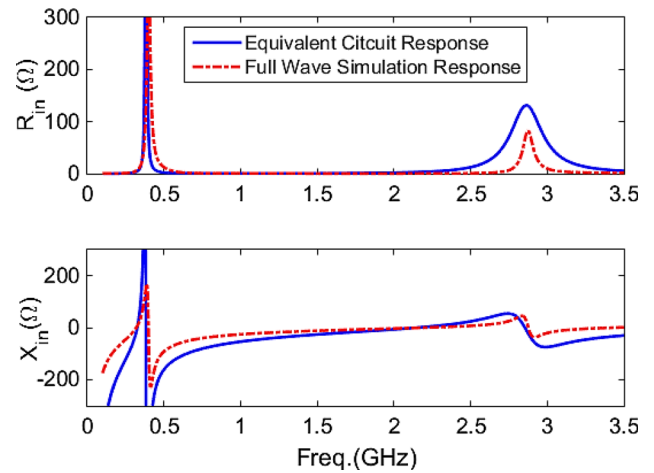

Fig. 8 Response of both dual band equivalent circuit and full wave simulation after taking the medium loading into account. Full wave simulation response has a lower resistance value at resonance than equivalent circuit response due to other dielectric losses that have been neglected in the circuit analysis
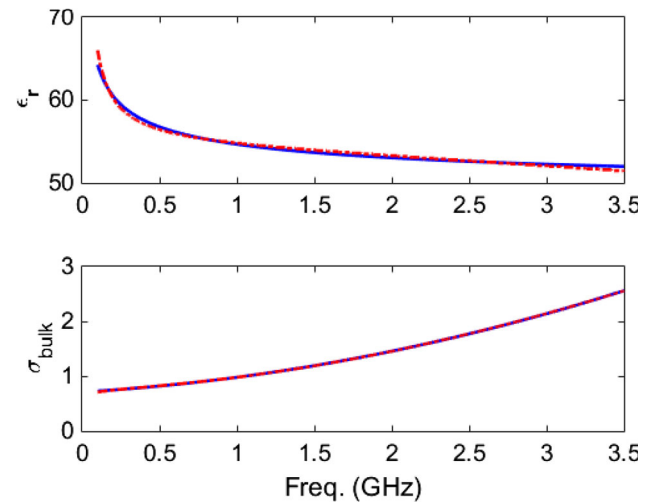

Fig. 9 Electrical properties of the immersing medium

5 Tri-band ECLA

The triple band implanted antennas were suggested in Das and Yoo (2017); Shakib et al. 2014; Mahfouz et al. 2018) to improve the implanted system performance. The bands occupy both MICS and ISM for biomedical data telemetry and implanted system control, respectively. The third band is used for wireless power transfer which guarantees the operational continuity in addition to less batteries usage that helps reducing the overall system size.

Table 3 Radii of the approximate circular loops corresponds ECLA radiators

Radius	Value (mm)	Description
a_1	12.9896	Equivalent radius for biocompatible coating material (low band)
a_2	$0.35 \times a_1$	Radius of the equivalent insulating material (high band)
b_1	8.1173	Equivalent radius for low band loop radiator
b_2	1.8	Equivalent radius for high band loop radiator

Fig. 10 Tri-band ECLA dimensions with the same substrates used in the dual-band design **a** elevation view and **b** top view

(a)

(b)
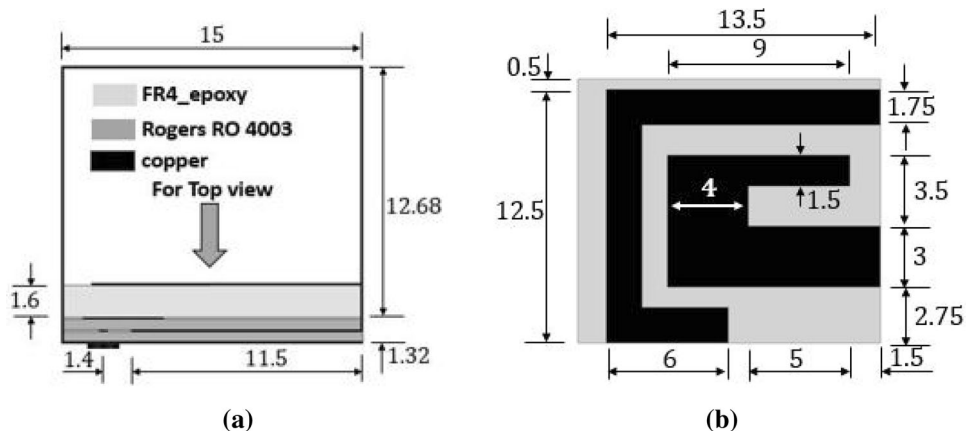
The geometry of the tri-band ECLA is depicted in Fig. 10. For the readers' knowledge, tri-band ECLA was proposed for the first time in Mahfouz et al. (2018) with slight different design without experimental verification and sufficient explanation. It consists of the loop body which is responsible for MICS band excitation and two strips branched from the loop body.
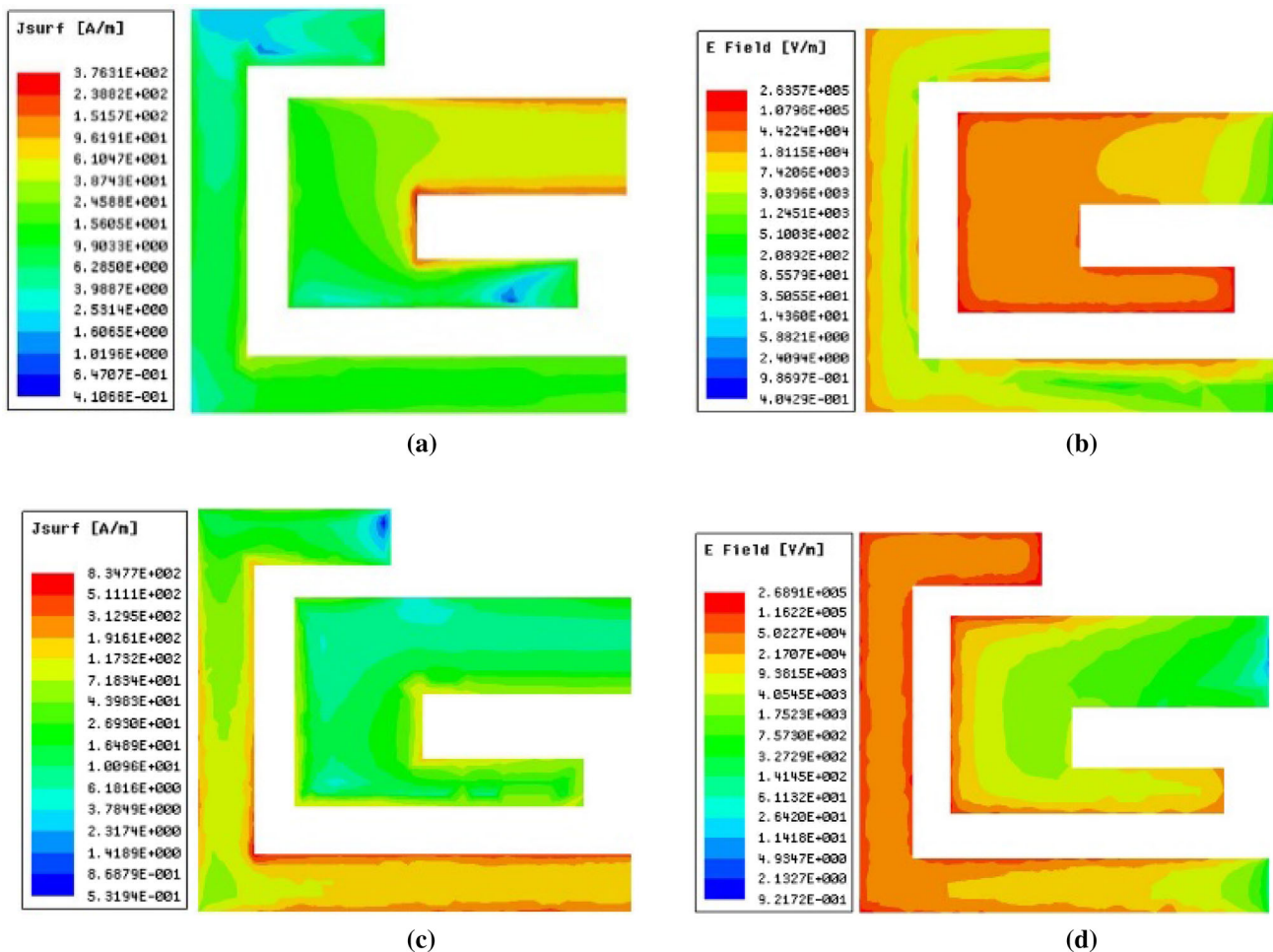

(a)

(b)

(c)

(d)

Fig. 11 Surface current and normal electric field distributions for ISM band in both (**a**), (**c**) and for WMTS band in both (**b**), (**d**). These distributions are at zero phase which have been taken from the bottom surface of the strips with logarithmic scale colormap. For clearer view enlarge page
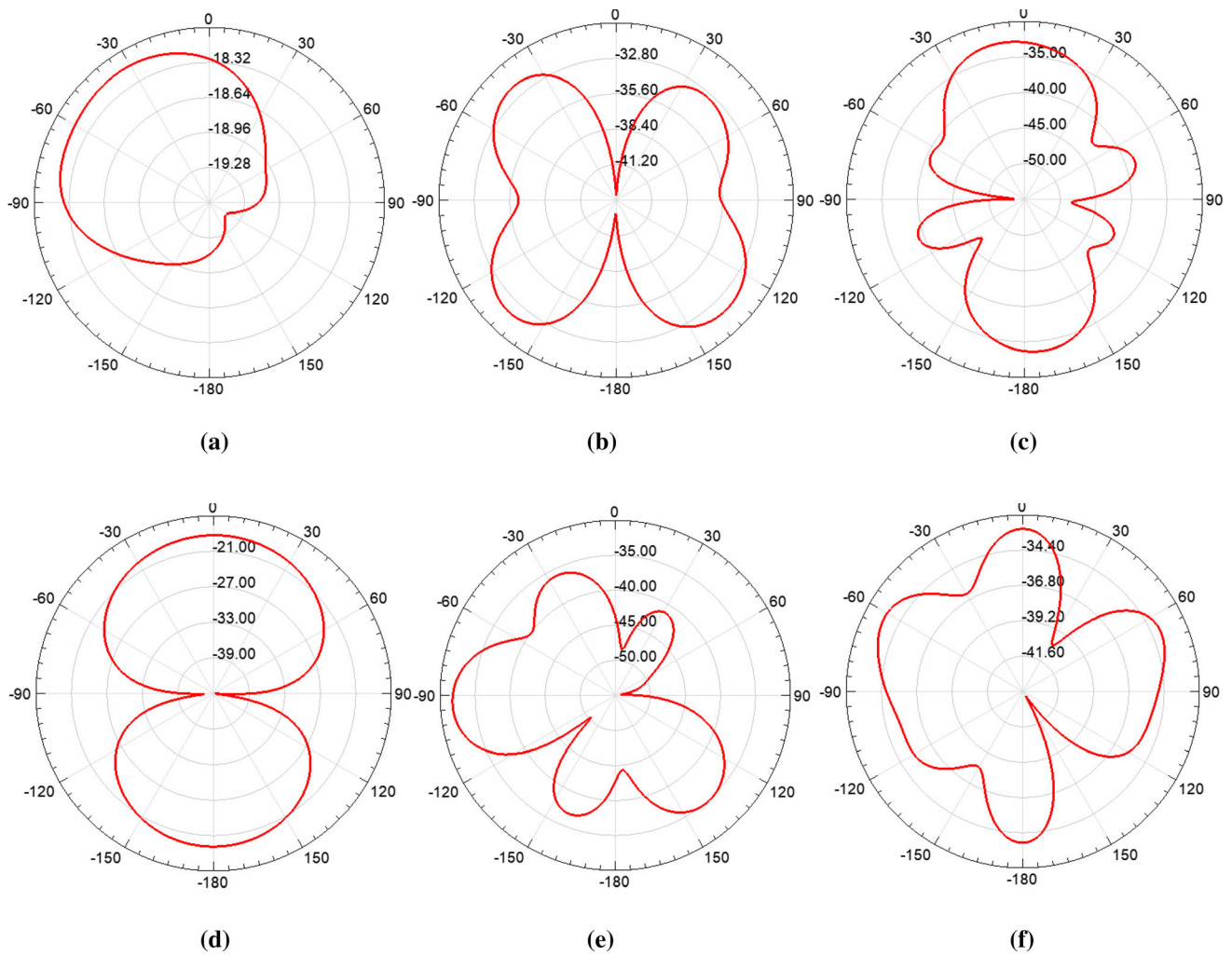
Fig. 12 Polar radiation patterns for the proposed antenna in the loop plane *yzplane* for the group (**a**), (**b**) and (**c**) and in *xzplane* for the group (**d**), (**e**) and (**f**). **a** and **d** patterns correspond MICS whereas **b** and **e** for WMTS and finally the ISM patterns are displayed in **c** and **f**

Table 4 Dispersion parameters for some human tissues according to proposed model

0.1 < f < 3.5 GHz			
Tissue	Muscle	Colon	Skin wet
a	1.298e + 04	7.108e + 05	1. 06e + 06
b	− 0.3605	− 0.544	− 0.5768
c	47.29	48.26	38.72
q_1	1.041e-19	0.9177e-19	0.7011e-19
q_2	1.647e-10	3.2e-10	2.556e-10
q_3	0.7094	0.7079	0.5493

Surface current distribution on these strips reveals that the excitation of the ISM band has occurred due to the short strip whereas the tall strip excited WMTS band. Returning to the equivalent circuit of the ECLA, such antenna is modeled by three resonance circuits in addition to coupling circuit where each strip represents a parallel resonance circuit. The circuit elements can be extracted using (3) and (4) but the dimensions must be plugged in according to the surface current and the normal electric field distributions on the strips as illustrated in Fig. 11 because they no longer take uniform distributions. By neglecting coupling effects between the two strips, it is noted that the surface current is maximum at the start of the strip whereas the normal electric field is maximum at the strip end for both high bands. The circuit parameters values for the strip excites ISM band are 2.2341(nH) considering strip area 6mm × 3mm and 1.998(pF) considering it consists of three parts of areas 5mm × 1.5mm, 6.5mm × 4mm and 3mm × 1mm. The corresponding resonance frequency for these circuit parameters equals 2.38 GHz. Following the same steps, the circuit parameters of the WMTS strip are 8.5874(nH) and 1.8212(pF) correspond resonance frequency equivalent to
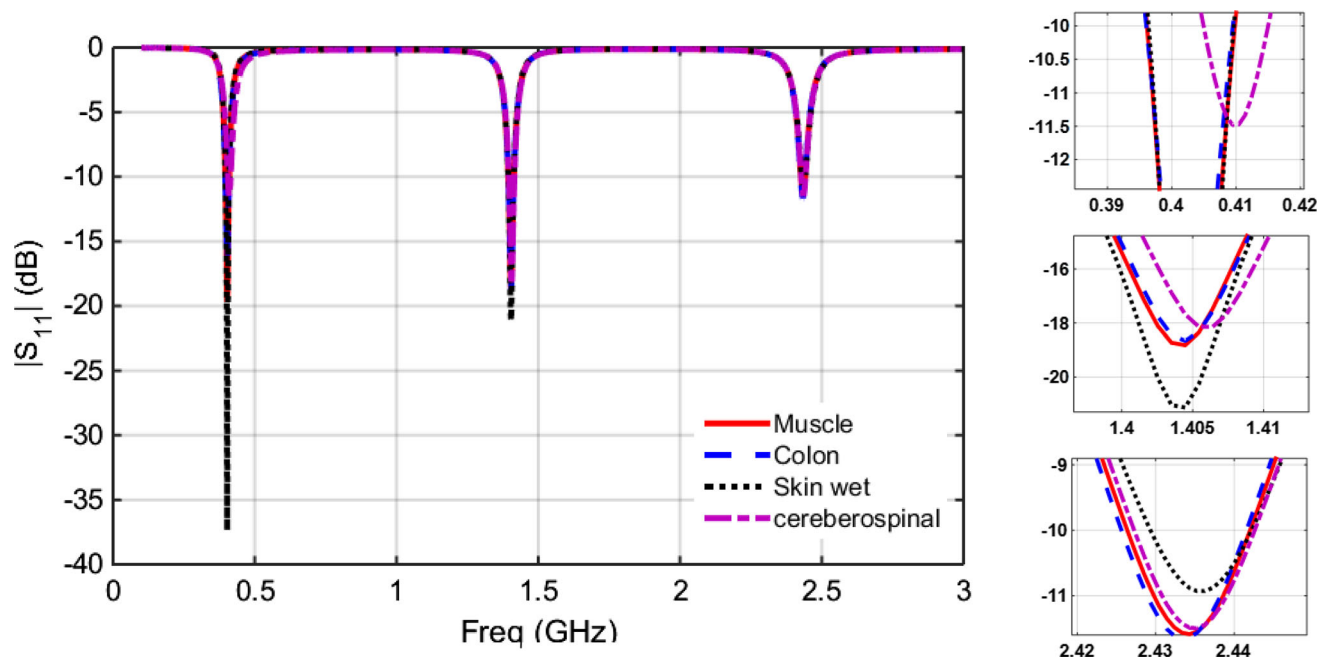
Fig. 13 A detuning study of the proposed antenna in different human tissues

1.27 GHz. Finally, the loop body is modeled by inductance value equals 12.51nH with a matching capacitance value 10.92(pF). The corresponding resonance frequency is 0.42 GHz. It is clear that there is a slight drift between the resonance frequencies calculated using the full wave analysis and the deduced resonance frequencies from the equivalent circuit. There are two reasons for that drift, the first, which is the most important, is considering each resonance element in the antenna structure does not affect other elements. Although the weak correlation between the three radiators but there is a slight dependence led to such drift. The correlation is measured by the frequency shift amount if each radiator is tested separately. The uniform distributions assumptions are considered as a second reason.

6 Results and experimental work

The antenna is simulated using High Frequency Simulator structure (HFSS). The immersing medium was a muscle phantom with electrical properties shown before in Fig. 9. They are expressed as a function in frequency using the following interpolating model:

$$\epsilon_r = af^b + c \tag{11a}$$

$$\sigma = q_1 f^2 + q_2 f + q_3 \tag{11b}$$

where $a, b, c, q_1, q_2, and q_3$ are constants depends on tissue type, f represents the frequency, ϵ_r, σ represent the relative dielectric constant and the bulk conductivity of the

phantom successively. This model is found a very good interpolating model to fit the tabulated data in Dielectric Properties of Body Tissues (1987) in simpler manner than other models. The following table shows the values of these constants for some human tissues as an example.

The simulated tri-band ECLA peak realized gains are $-18, -30,$ and -33.3 dBi for the three bands, respectively. It worth to mention that the antenna is simulated in a muscle phantom with size $100 \times 100 \times 100mm^3$ since the calculated gains consider the losses in the medium so if the size of the dissipative phantom increases the radiated power outside the phantom decreases and consequently the calculated gain also decreases. The calculated peak SAR value for the MICS band is 11.59 W/Kg, averaged on 10 gm, which is near from the dual band design (Akbarpour and Somayyeh 2017) whereas the ISM peak SAR value is 49.57 W/Kg which is the double of the aforementioned design (Akbarpour and Somayyeh 2017). This increment because the strip excites this band is narrower than it in Akbarpour and Somayyeh (2017) which leads to a more electric field concentration causes an increment in SAR value. The SAR is 43.09 W/Kg for the WMTS band. The simulated radiation patterns for the three bands are shown in Fig. 12 in the loop plane (yz plane) and orthogonal plane (xz plane). The pattern of the MICS band is omnidirectional in the loop plane and has a null in the loop center which are the same radiation characteristics of the magnetic dipole. It is noted that the patterns of both WMTS and ISM are different from the loop pattern characteristic since

Fig. 14 Tri-band ECLA Fabrication and Testing. **a** Loop with electric coupling for MICS band excitation in addition to the two strips for WMTS & ISM bands excitation. **b** The overall antenna shape after fixing the upper bands part in the loop body. **c** covering the antenna by 3 mm thickness Teflon sheet. **d** Testing the antenna in a solution mimics the muscle tissue
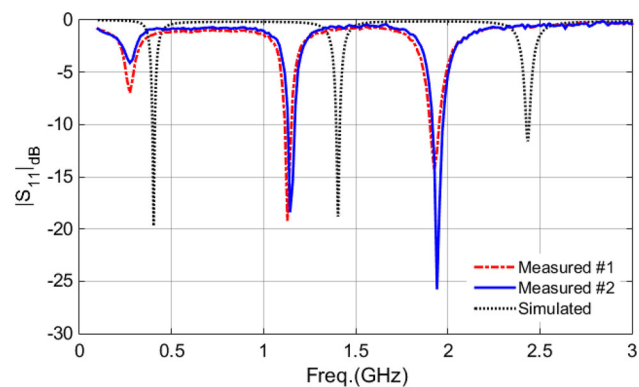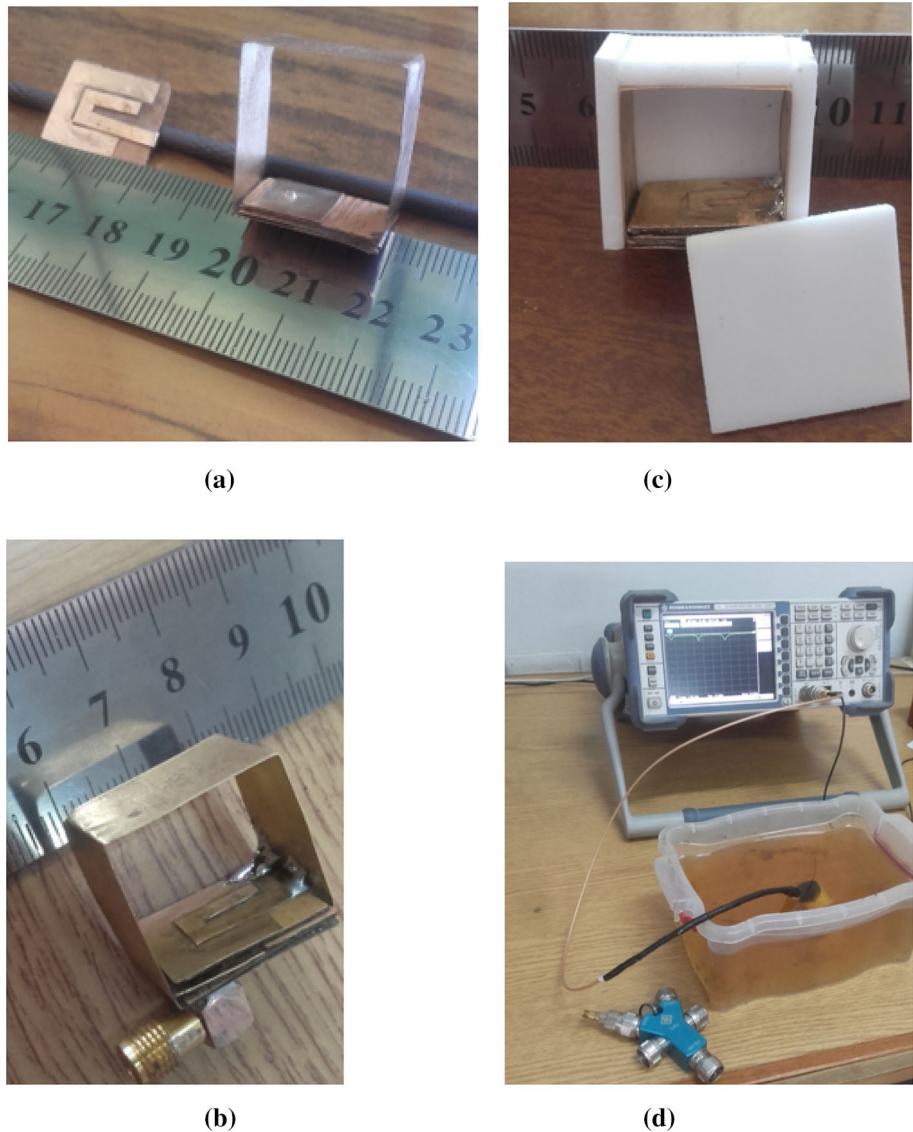

(a)

(c)

(b)

(d)

Fig. 15 Reflection coefficient for the fabricates Prototypes (solid and dotted Lines) and Simulated (dash-dotted Line). A notable shift between the simulated response and the measured response because of the large size of the fabricated prototypes. These are the less size models which we were able to fabricate manually using our available facilities

the major radiators for these bands do not take a loop shape as explained in Sect. 5.

A detuning study is performed to confirm that the proposed antenna is robust against electrical properties changes. The antenna is simulated in different human tissues with dispersion curves illustrated in Table 4. The relative permittivity changes from 50 to 71, 44.3 to 67.15 and 42.8 to 66.18 at the three resonance frequencies, respectively whereas the bulk conductivity varies between 0.66 and 2.24 S/m at 0.403 GHz, 1.05 to 2.67 S/m at 1.4 GHz and 1.59 to 3.44 S/m at 2.44 GHz. The magnitude of the reflection coefficient is illustrated in Fig. 13. It is noted that there is no notable shift from the resonance position but the matching levels changed since the dissipation varies from tissue to another. Also, the dissipation varies from frequency to another.

The tri-band ECLA has been fabricated using a copper sheet with thickness 0.18 mm and a wooden slab from Formica with thickness 0.7 mm and relative dielectric constant ranges from 1.4 to 2.9 as shown in Fig. 14. The tested antenna has larger size than the simulated model since it was fabricated manually due to lack of precise machinery the matter that caused a notable shift in the resonance frequencies as depicted in Fig. 15. It is worth to mention that the magnitudes of the reflection coefficients of the fabricated prototypes do not have a uniform scale from the simulated tri-band ECLA response, i.e. the shift at lower resonance frequency does not equal the shift at higher frequencies or even related to each other by a constant scaling factor.

The reason of this variance between both curves, simulated and measured, is the fabrication tolerance difference for each resonance part. The dependence of the resonance parts is weak which is considered one of the advantages of this model. In other words, the ratio between the fabricated loop dimensions and the simulated loop dimensions does not equal the ratio between the fabricated strip dimensions and simulated strip dimensions. A second prototype was manually fabricated and tested using Rhode & Schwarz ZVL6 VNA to guarantee robustness against process variation. Its response is shown in Fig. 15.

7 Conclusion

An equivalent circuit for the ECLA was introduced for the single and dual band models. It related the dimensions with the circuit parameters the matter that facilitates the design of the triple band ECLA which used for the data telemetry, WPT and system control. The impedance responses of the fabricated models are shifted down since they have larger size than the simulated antenna. The loading of the dissipative medium is taken into account for each resonance frequency created by a loop radiator. The losses of the substrates and biocompatible coating are neglected so the responses of the full wave analysis have lower maximum value than the equivalent circuit response. The proposed antenna has been simulated in different human tissues to check its robustness against detuning effect. Two models have been fabricated and tested as a proof of concept.

References

Akbarpour A, Somayyeh C (2017) Dual-band electrically coupled loop antenna for implant applications. IET Microwaves Antennas Propagat 11(7):1020–1023

Balanis CA (2016) Antenna theory: analysis and design. John Wiley and Sons, Hoboken

Chao R-Y, Chung K-S (1994) A low profile antenna array for underground mine communication. In: Proceedings of ICCS'94. Vol. 2. IEEE

Chen C-L, King R (1963) The small bare loop antenna immersed in a dissipative medium. IEEE Trans Antennas Propagat 11(3):266–269

Das R, Yoo H (2017) A multiband antenna associating wireless monitoring and nonleaky wireless power transfer system for biomedical implants. IEEE Trans Microwave Theory Techn 65(7):2485–2495

Dielectric Properties of Body Tissues (1987) Institute for Applied Physics, "Nello Carrara" -Florence (Italy) [Online]. Available: http://niremf.ifac.cnr.it/tissprop/htmlclie/htmlclie.php

Geyi W (2003) A method for the evaluation of small antenna Q. IEEE Trans Antennas Propag 51(8):2124–2129

Ghosh D, Moon H, Sarkar TK (2008) Design of through-the-earth mine communication system using helical antennas. In: 2008 IEEE Antennas and Propagation Society International Symposium. IEEE

Hall PS, Hao Y (2006) Antennas and propagation for body-centric wireless communications. Artech House, Norwood, MA

Hosseini M, Zhu G, Peter Y-A (2007) A new formulation of fringing capacitance and its application to the control of parallel-plate electrostatic micro actuators. Analog Integr Circ Sig Process 53(2–3):119–128

Ibraheem AAY, Manteghi M (2014) Performance of an implanted electrically coupled loop antenna inside human body. Prog Electromagn Res 145:195–202

Khan AS (2014) Microwave engineering: concepts and fundamentals. CRC Press

Mahfouz M, IbrahimAAY, Haraz OM (2018) Triple-band electrically coupled loop antenna (ECLA) for biomedical implantation purposes. In: 2018 35th National Radio Science Conference (NRSC). IEEE

Manteghi M (2013) Electrically coupled loop antenna as a dual for the planar inverted-f antenna. Microw Opt Technol Lett 55(6):1409–1412

Manteghi M, Ibraheem AAY (2014) On the study of the near-fields of electric and magnetic small antennas in lossy media. IEEE Trans Antennas Propagat 62(12):6491–6495

Ramo S, Whinnery JR, Van Duzer T (2008) Fields and waves in communication electronics. John Wiley & Sons

Shakib M et al (2014) Design of a tri-band implantable antenna for wireless telemetry applications. In: 2014 IEEE MTT-S

International Microwave Workshop Series on RF and Wireless Technologies for Biomedical and Healthcare Applications (IMWS-Bio2014). IEEE

Turner RW (1959) Submarine communication antenna systems. Proc IRE 47(5):735–739

Wait JR (1957) Insulated loop antenna immersed in a conducting medium. J Res NBS 59(2):133–137

Wheeler HA (1947) Fundamental limitations of small antennas. Proc IRE 35(12):1479–1484

Yan L, Waynert JA, Sunderman C (2013) Measurements and modeling of through-the-earth communications for coal mines. IEEE Trans Ind Appl 49(5):1979–1983